ADVANCED ENERGY MATERIALS
www.advenergymat.de

Perylene Diimide Trimers Based Bulk Heterojunction Organic Solar Cells with Efficiency over 7%

Ningning Liang, Kai Sun, Zhong Zheng, Huifeng Yao, Guangpeng Gao, Xiangyi Meng, Zhaohui Wang, Wei Ma,* and Jianhui Hou**

Polymer solar cells (PSCs) have been widely investigated for their light weight, low cost, and the capability to fabricate the flexible devices.[1,2] Fullerene derivatives have been broadly used in PSCs due to the ultrafast photo-induced electron transfer between the fullerene acceptors and polymer donors.[3–9] In order to improve photovoltaic performance of bulk heterojunction (BHJ) PSCs, much effort has been devoted to investigate the correlations among the chemical structures of donors and acceptors, device architecture, BHJ morphology and so on.[10–12] The power conversion efficiencies (PCEs) of PSCs based on fullerene acceptors have exceeded 10%.[13–15] However, fullerene derivatives have several drawbacks, including poor light absorption, difficulty in tuning the energy level by changing the chemical structure, and high cost production.[16] Therefore, it is an important topic to explore non-fullerene acceptors to promote the further development of PSCs.

Among the non-fullerene acceptors, perylene diimide (PDI) derivatives have attracted significant attention and exhibited great potential due to their good electron-accepting ability, high electron mobility, especially their highly tunable electronic energy levels by chemical modification.[17,18] As known, PDI-based small molecule acceptors have a strong tendency to form microscale or sub-microscale aggregations in BHJ active layers, which leads to strong geminate or bimolecular recombination and thereby limits the photovoltaic performance of PSCs.[19,20] To solve this problem, varied methods have been employed to suppress the aggregation effect of PDIs. A frequently used method to disrupt the planarity of PDIs and thus to reduce the aggregation tendency is to link two PDI units via their bay positions with different linkage units.[21,22] For example, SF-PDI$_2$ was a highly twisted PDI derivative using spiro-fluorene (SF) bridge as the linkage and when it was blended with a suitable donor, PffBT4T-2DT, to fabricate PSCs devices, an impressively high open circuit voltage (V_{oc}) of 0.98 V and a PCE of 6.3% were achieved.[23] Recently, a new electron acceptor named as Sdi-PDI-S, was obtained, by introducing two thiophene units in the bay positions of Sdi-PDI, and a high PCE of 7.16% was obtained in device.[24] A helical molecular semiconductors, hPDI4, consisting of helical conjugated PDI tetramers was reported as an electron acceptor, and the PCE of the solar cell device reached 8.3%.[25] In addition, PDI-based polymers and 3D small molecules were also designed and applied in PSCs.[26–28] According to the reported work, the method to tune the torsion angel between adjacent bay-linked PDI units has been regarded as an effective method for alleviating the aggregation tendency of PDI-based acceptors.

Another effective method to disrupt the planarity of PDIs is to link two PDI units via the imide position.[29] In this case, the PDI units are oriented perpendicularly to each other through an N—N bond, hence we named these PDIs derivatives as H-*n*-PDI, where *n* is the number of repeat PDI units. A 2D conjugated benzodithiophene (BDT)-based polymer, PBDT-TS1, was used as the polymer donor and an N—N-linked PDI derivative (PPDI) as the acceptor to prepare the PSC devices and obtained a PCE of 5.4%;[30] in a more recent work, the devices based on PTB7-Th:PPDI showed a PCE as high as 6.4%.[31] Obviously, the H-*n*-PDI-based devices have similar photovoltaic performance to those of the bay-position linked PDIs. In addition, the synthetic route of H-*n*-PDIs is quite simple and this type of PDI derivatives have many active sites (four bay positions for one PDI unit) for further modification, which is helpful for further fine tuning their energy levels. Furthermore, the absorption intensity can be enhanced with the increasing number of *n* in H-*n*-PDIs molecules.[32,33] Therefore, although H-*n*-PDI materials rarely have been applied in PSCs to date, they have shown great potential to be effective electron acceptors.

In this work, a new PDI-based acceptor named H-tri-PDI was reported. As shown in **Figure 1**a, this molecule is composed of three PDI units that are connected together via imide positions. H-tri-PDI exhibits high extinction coefficient and a complementary absorption spectrum with the PBDT-TS1 donor in visible region; also the blend of H-ri-PDI and PBDT-TS1 possesses an appropriate energy level alignment. What's more, the BHJ active layer based on PBDT-TS1:H-tri-PDI has favorable morphology, which facilitates charge separation in the BHJ blend of H-tri-PDI and PBDT-TS1. The device based on PBDT-TS1:H-tri-PDI shows a PCE as high as 7.25% with a short circuit current density (J_{sc}) of 16.5 mA cm^{-2}, which is the highest

N. Liang, K. Sun, Z. Zheng, H. Yao, G. Gao, Prof. Z. Wang, Prof. J. Hou
Institute of Chemistry
Chinese Academy of Sciences
Beijing 100190, China
E-mail: wangzhaohui@iccas.ac.cn; hjhzlz@iccas.ac.cn
N. Liang, K. Sun, Z. Zheng, H. Yao, G. Gao
University of Chinese Academy of Sciences
Beijing 100049, China
X. Meng, Prof. W. Ma
State Key Laboratory for
Mechanical Behavior of Materials
Xi'an Jiaotong University
Xi'an 710049, China
E-mail: msewma@mail.xjtu.edu.cn

DOI: 10.1002/aenm.201600060

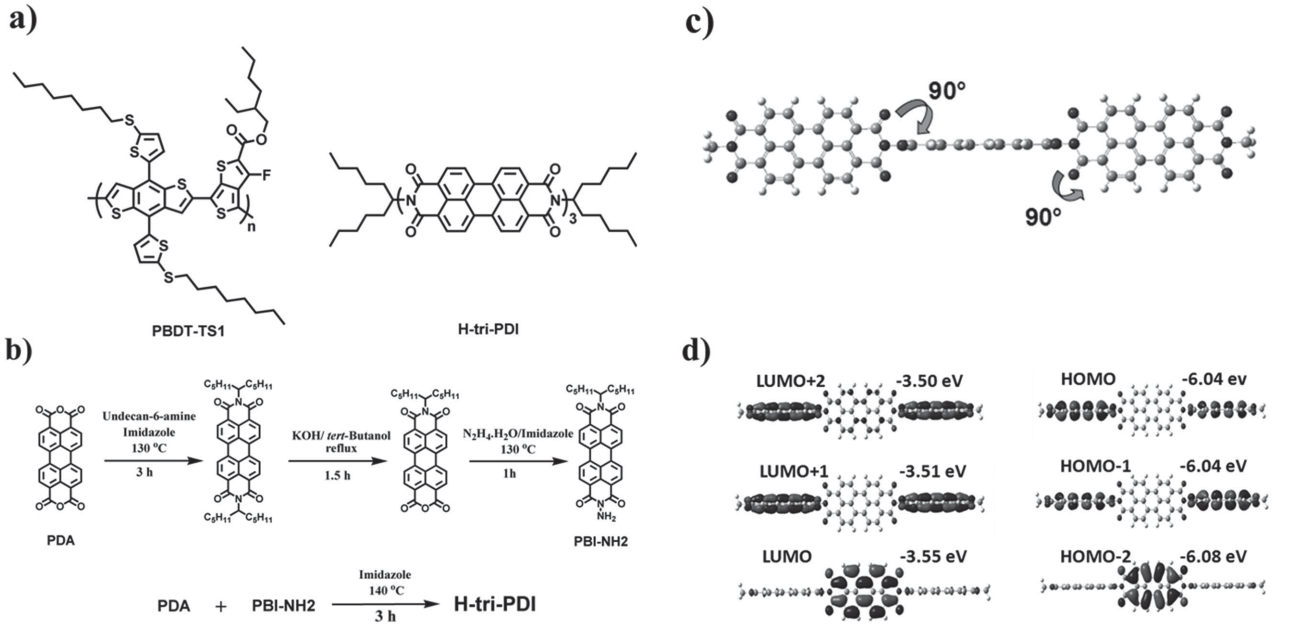

Figure 1. a) Chemical structures of the donor PBDT-TS1 and acceptor H-tri-PDI. b) Synthetic routes of H-tri-PDI. c) Optimized geometry of H-tri-PDI. d) Theoretical calculations of H-tri-PDI using DFT calculations at the B3LYP/6-31G (d, p) level.

value reported for non-fullerene PSCs based on H-*n*-PDI so far. These results demonstrate that H-tri-PDI molecules have great potential to be an electron acceptor and the method of connecting multiple PDI units via the imide position can be used to further develop of PDI-based acceptor materials.

The synthetic route of H-tri-PDI is shown in Figure 1b. PBI-NH2 was synthesized according to the literature.[24,30] Then, H-tri-PDI was synthesized in 28% yield by combining perylene dianhydride, PBI-NH2, and imidazole at 140 °C under nitrogen for 3 h. It was fully characterized with ^{1}H and ^{13}C nuclear magnetic resonance (NMR) spectroscopy (see Supporting Information) and can be easily dissolved into chlorobenzene (CB), *o*-dichlorobenzene (*o*-DCB), and chloroform (CF) at room temperature.

Density functional theory (DFT) calculations at the B3LYP/6-31G (d, p) level were used to get the optimized geometry and the electronic structures of the molecular orbitals of H-tri-PDI. As shown in Figure 1c, the adjacent PDI units are perpendicular to each other. More interestingly, as shown in Figure 1d, although the distribution of lowest unoccupied molecular orbital (LUMO) surface is different from those of the LUMO+1 and LUMO+2 surfaces, these three LUMO orbitals have the almost same energy levels, i.e., −3.50, −3.51, and −3.55 eV for LUMO, LUMO+1, and LUMO+2, respectively, and the similar phenomenon can be observed in the highest occupied molecular orbital (HOMO) levels as well. These results indicate that as an acceptor material, H-tri-PDI has three LUMO levels with similar ability to accept electrons from donor and the three HOMO levels can donate holes to the donor material.

The ultraviolet visible (UV–vis) absorption spectra of H-tri-PDI in dilute chloroform solution (10^{-5} M) and solid thin film are shown in **Figure 2**a. It reveals that H-tri-PDI material has narrow multiple absorption peaks throughout the 400–550 nm range and a main peak at 537 nm with $\varepsilon_{max} = 2.8 \times 10^5$ $M^{-1}cm^{-1}$(Figure S4, Supporting Information). The absorption peak of the pure H-tri-PDI is slightly red shifted by 10 nm from solution to solid film, which demonstrates that there were enhanced intermolecular π–π interactions in solid state. The absorption spectrum of the H-tri-PDI film has an absorption edge (λ_{edge}) at 598 nm, corresponding to the optical bandgap (E_g) of 2.09 eV. In addition, Figure 2b also shows that absorption spectrum of H-tri-PDI is complementary to that of PBDT-TS1, so the blend of H-tri-PDI:PBDT-TS1 can absorb solar light from visible and near-infrared region.

Electrochemical cyclic voltammetry (CV) was employed to measure the energy levels of H-tri-PDI and PBDT-TS1. Similar to fullerene derivatives, H-tri-PDI has several reduction waves. As shown in Figure 2c, the three onset reductions (φ_{red}) and all of the onset oxidations (φ_{ox}) of H-tri-PDI measured in solution are higher than those of PBDT-TS1, respectively. The onsets of reduction and oxidation potentials versus Fc/Fc^+ are −0.87 and 1.21 V, respectively. Thus, according to the onset reduction and oxidation potentials, the LUMO and HOMO levels of H-tri-PDI are estimated to be −3.93 and −6.01 eV, respectively, assuming that the potential of Fc/Fc^+ is 4.8 eV below vacuum.[34] According to the LUMO and HOMO levels of PBDT-TS1 (LUMO = −3.52 eV, HOMO = −5.33 eV),[35] the offset between the LUMO of the donor and the acceptor is calculated to be 0.41 eV, as shown in Figure 2d. Those results demonstrate that the three LUMO orbitals of H-tri-PDI can accept the electrons from PBDT-TS1 and the three HOMO levels can give holes to the donor, implying that the property of H-tri-PDI could make the charge separation occur efficiently. As shown in Figure 2e, H-tri-PDI displays a strong fluorescence emission, but is completely quenched by the PBDT-TS1, indicating that the non-radiant electron transfer occurs efficiently at the interface of H-tri-PDI and PBDT-TS1.

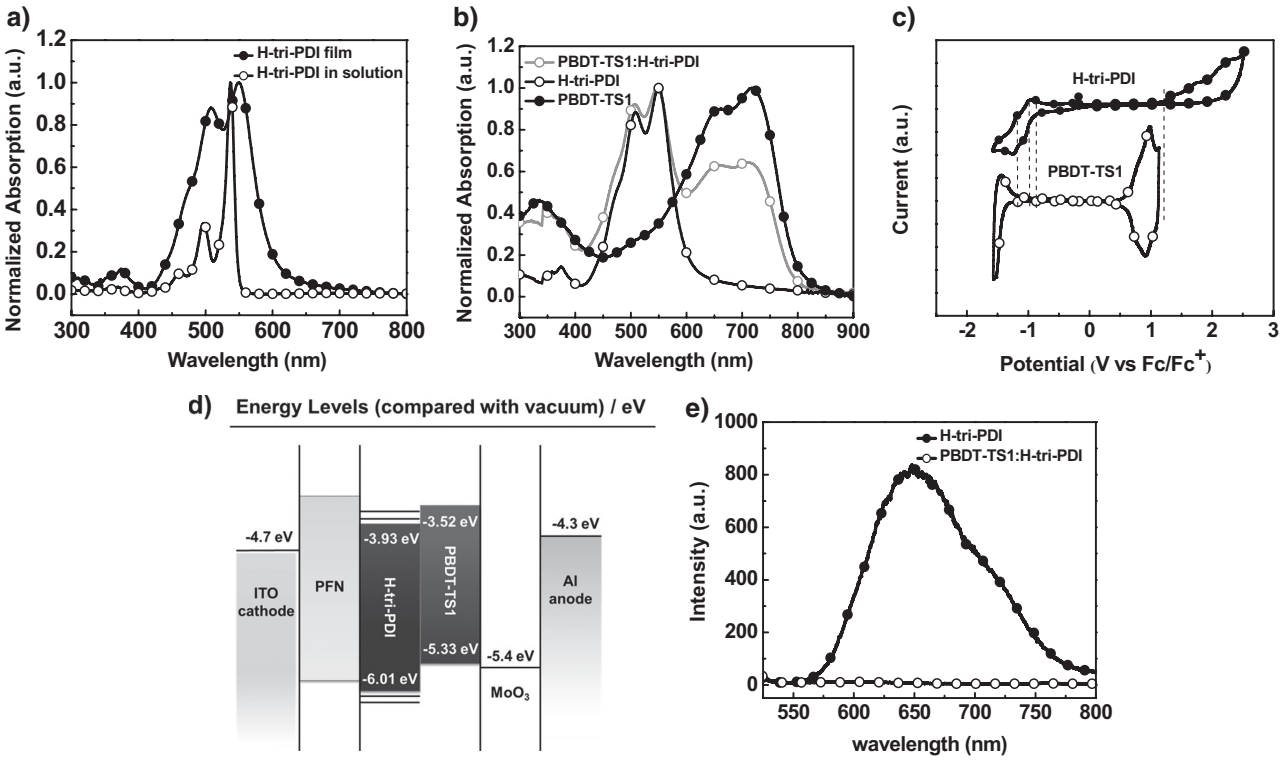

Figure 2. a) Normalized UV absorption spectra of H-tri-PDI solution and film on quartz substrate. b) Normalized UV absorption spectra of H-tri-PDI, PBDT-TS1, and PBDT-TS1:H-tri-PDI blend (1:1 w/w, PBDT-TS1 concentration is 10 mg mL^{-1}). c) Cyclic voltammetry plot of H-tri-PDI and PBDT-TS1. d) Energy level diagram of the inverted device structure. e) Fluorescence spectrum of the pure acceptor H-tri-PDI and the PBDT-TS1:H-tri-PDI blend films; the excitation wavelength was 508 nm.

In order to assess the photovoltaic properties of H-tri-PDI, photovoltaic devices were prepared with an inverted device structure of ITO/PFN/PBDT-TS1:H-tri-PDI/MoO_3/Al, where the thicknesses of PFN and MoO_3 were referred to previous literature.[12,36,37] According to the literature,[37] the PFN can reduce the work function of the ITO from 4.7 to 4.1 eV and the modified ITO can form ohmic contact with the BHJ active layer, which can facilitate the charge transport and collection. Using CB as the main solvent, we studied the effect of the donor and acceptor weight ratio on device performance. The photovoltaic parameters of PBDT-TS1:H-tri-PDI devices at different donor/acceptor ratios are summarized in **Table 1** and the corresponding current–density/voltage (*J*–*V*) curves and the external quantum efficiency (EQE) spectra are shown in Figure S6 in the Supporting Information. The solar cell devices with a weight ratio of 1:1 show the best performance with a V_{oc} of 0.714 V, a J_{sc} of 14.9 mA cm^{-2}, a fill factor (FF) of 54.6%, resulting in a PCE of 5.81%.

To further improve device performance, di-phenyl ether (DPE) was used as the additive to optimize the BHJ active layer morphology on the basis of 1:1 donor/acceptor ratio. The device parameters with different DPE amount are summarized in **Table 2** and **Figure 3**a. When the amount was 7%, the device showed a highest PCE of 7.25% with a V_{oc} of 0.732 V, a J_{sc} of 16.52 mA cm^{-2} and a FF of 60.3%. When we increased the active layer thickness by slowing down the spinning speed for coating the active layers, a higher J_{sc} of 17.11mA cm^{-2} was recorded, which is comparable with that obtained in the PBDT-TS1:PC_{71}BM-based device.[35] As shown in Table S1 in the Supporting Information, the PCE of devices dropped to 7.08%, 6.88%, 3.98%, respectively, when the active layer thickness increased to 110, 180, 290 nm.

As shown in Figure 3b, the current density integrated from the EQE spectrum has a small difference with J_{sc} measured from the corresponding *J*–*V* curves. The EQE value in the range of 460–550 nm exceeds 70% with the maximum of 75%, which

Table 1. Device performance parameters of PSCs based on PBDT-TS1:H-tri-PDI BHJ at different donor/acceptor ratios under AM 1.5G illumination at 100 mW cm^{-2}.

PBDT-TS1:H-tri-PDI [wt/wt]	V_{oc} [V]	J_{sc} [mA cm^{-2}]	FF [%]	PCE [%]	Thickness [nm]
1.5:1	0.692	12.11	53.02	4.44	90
1:1	0.714	14.92	54.57	5.81	90
1:1.5	0.702	14.24	48.50	4.58	92

Table 2. Device performance parameters of PSCs based on PBDT-TS1:H-tri-PDI BHJ with different DPE amount under AM 1.5G illumination at 100 mW cm^{-2}.

DPE [by volume, %]	V_{oc} [V]	J_{sc} [mA cm^{-2}]	FF [%]	PCE [%]	Thickness [nm]
0	0.714	14.92	54.57	5.81	95
4	0.726	15.13	59.49	6.53	90
7	0.732	16.52	60.03	7.25	85
10	0.745	14.10	61.96	6.33	86

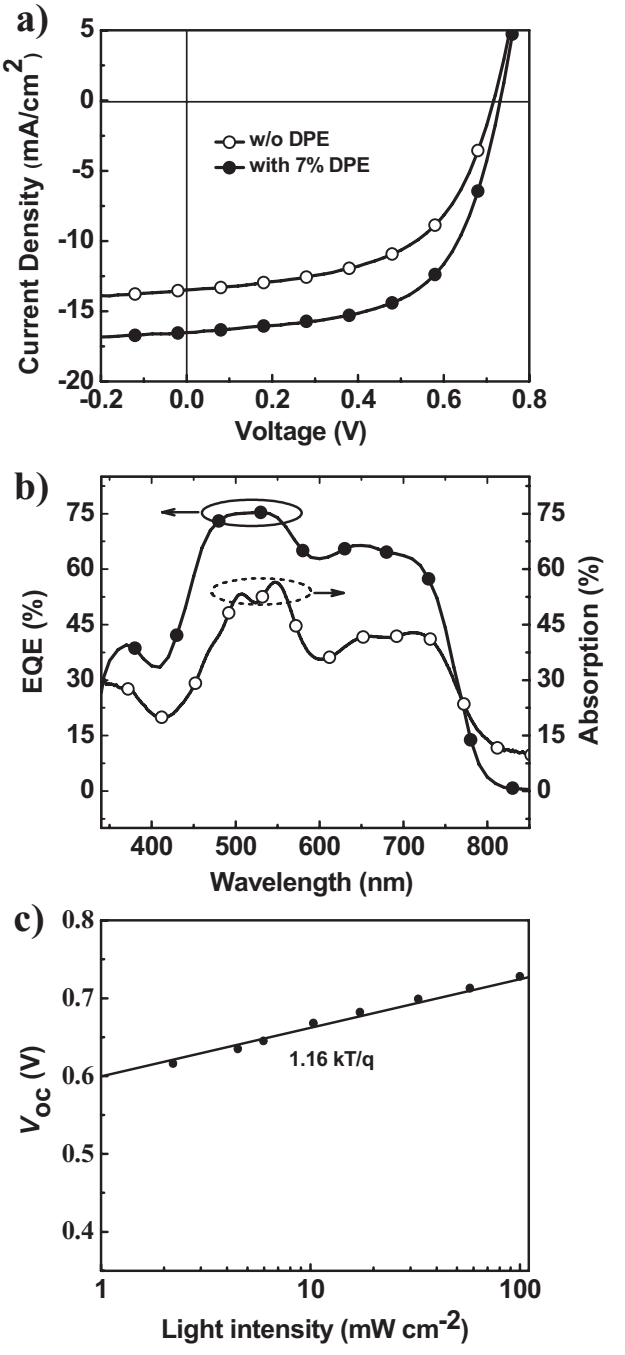

Figure 3. a) *J–V* curves of solar cell devices without and with 7% DPE. b) EQE spectrum and the absorption spectrum of solar cell device with 7% DPE. c) V_{oc} as a function of light intensity for PBDT-TS1:H-tri-PDI blend film with 7% DPE

is attributed to H-tri-PDI molecules, and the EQE value in the range of 550–740 nm surpasses 60% which is contributed by the PBDT-TS1 donor. In addition, the high and broad EQE curve is similar to the absorption curve in shape, indicating that the photo-generated excitons in the PBDT-TS1:H-tri-PDI BHJ active layer can be efficiently converted to free charges.

To investigate the carrier transport properties of the devices under the optimal condition, the space-charge-limited current (SCLC) method was used to measure the hole and electron mobilities with the device structure of ITO/PEDOT:PSS/PBDT-TS1:H-tri-PDI/Au and ITO/ZnO/PBDT-TS1:H-tri-PDI/Al, respectively. As shown in Figure S7 in the Supporting Information, the PBDT-TS1:H-tri-PDI blend films under the optimal conditions show asymmetric hole and electric mobilities with $\mu_{hole} = 1.2 \times 10^{-4}$ cm^2 v^{-1} s^{-1} and $\mu_{electron} = 1.4 \times 10^{-5}$ cm^2 v^{-1} s^{-1}.

As discussed in previous studies,[22,23,38] the dependence of *J–V* characteristics on light intensity can give information on the recombination loss of devices, especially on the geminate recombination and/or bimolecular recombination. In principle, if bimolecular recombination is dominant, the slope of V_{oc} versus ln(light intensity) will be kT/q. We investigated the relationship between V_{oc} and the light intensity of the device prepared under the optimal conditions. Obviously, the device shows a linear relationship with ln(light intensity) with a slope of 1.16 kT/q shown in Figure 3c. The result demonstrates that the bimolecular recombination in PBDT-TS1:H-tri-PDI active layer is mainly caused by the asymmetric charge carrier mobility. Although the V_{oc} varies with the change of light intensity, the *J–V* characteristics under different light intensity has the same dark *J–V* characteristics and the ideality factor (n_{id}) depending on the exact recombination mechanism can be calculated from the slope in the exponential increase regime in the dark *J–V* characteristics.[15] In addition, for a solar cell device with given active materials, a lower n_{id} means better device quality and hence better device performance.[38] Thus, we calculated the n_{id} from dark *J–V* characteristics of the device prepared under the optimal conditions and the n_{id} from Figure S8 in the Supporting Information is close to 1.85, which demonstrates that the recombination current is dominant, as observed in the result of *J–V* characteristics on light intensity in Figure 3c.

Atomic force microscopy (AFM) was used to investigate the morphologies of PBDT-TS1:H-tri-PDI blend films. As shown in **Figure 4**, the surface of PBDT-TS1:H-tri-PDI blend film without DPE is smooth and uniform with a root-mean-square (RMS) roughness of 0.78 nm; the RMS roughness of the blend surface is slightly increased to 1.03 nm when 7% DPE is added. It also can be observed from transmission electron microscopy (TEM) images. The addition of 7% DPE did not cause significant changes in phase separation. Both of the PBDT-TS1:H-tri-PDI

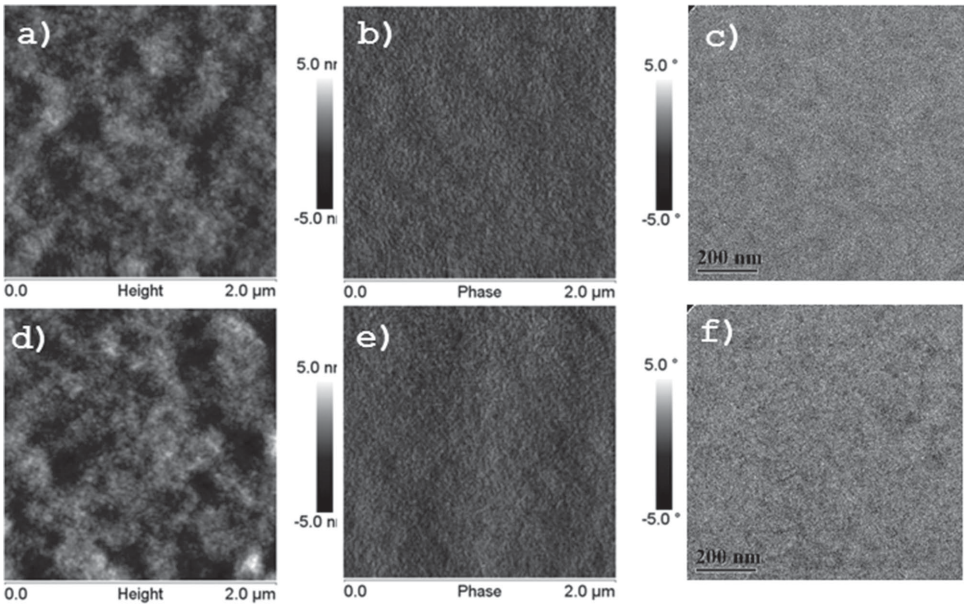

Figure 4. AFM a) height and b) phase images (2 μm × 2 μm) of PBDT-TS1:H-tri-PDI blend film without DPE and d) height and e) phase images (2 μm × 2 μm) of PBDT-TS1:H-tri-PDI blend film with 7% DPE. TEM images (scale bar = 200 nm) of PBDT-TS1:H-tri-PDI blend film c) without and f) with 7% DPE.

blend films with and without additive have favorable morphology and phase separation.

Successively, resonant soft X-ray scattering (R-SoXS) was used to investigate the spatial dimensions of phase separation (**Figure 5**a). The photon energy of 284.2 eV was chosen because of the highly enhanced contrast. The scattering profiles represent log-normal distribution function of spatial frequency, smode (smode = $q/2\pi$), which corresponds to the characteristic

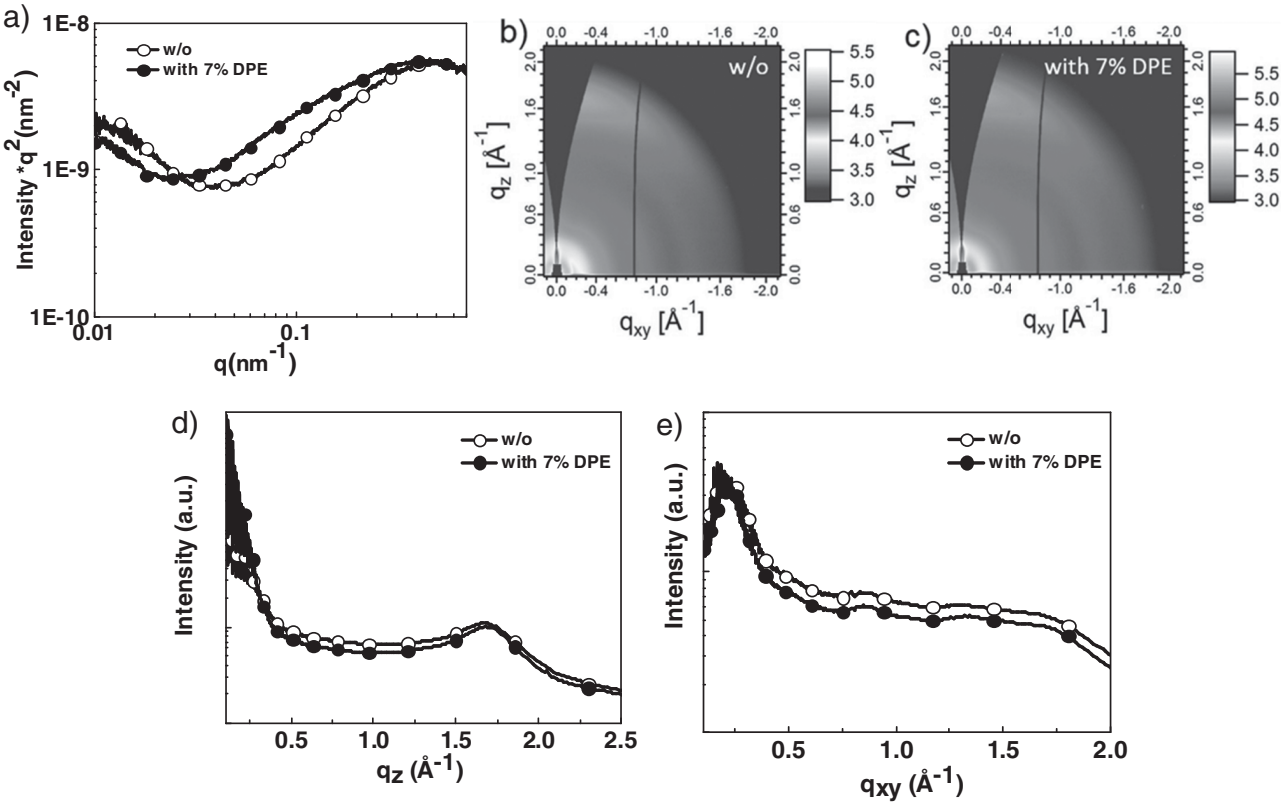

Figure 5. a) R-SOXS profiles for PBDT-TS1:H-tri-PDI blend film. 2D GIWAXS patterns of PBDT-TS1:H-tri-PDI blend films b) without additive and c) with 7% DPE. d) The out-of-plane and e) in-plane cuts of the corresponding 2D GIWAXS patterns.

mode length scale ξ, of the corresponding phase distribution in real space with $\xi = 1/\text{smode}$. The PBDT-TS1:H-tri-PDI blend film without additive shows the scattering with the ξ of ≈15 nm. When the additive DPE was added into the blend, the position of the scattering peaks does not change obviously, which indicates that the additive DPE had little influence on the domain size, which is in agreement with the TEM and AFM results. The relative domain purity can also calculated by R-SoXS via the integration of the scattering profiles. The blend films processed with 7% DPE as additive shows higher intensity, which suggests that domains are purer than the blend without additive. The purer domain is beneficial to exciton dissociation and reduce recombination.[39–41] These results can well explain why the blend films with 7% DPE as additive showed higher J_{sc} and FF.

To further investigate the influence of DPE on the molecular packing and the orientation of PBDT-TS1:H-tri-PDI blend films, we employed grazing incidence wide-angle X-ray scattering (GIWAXS).[42,43] As shown in Figure 5, the in-plane profiles of both blend films had same (h00) diffraction peaks, implying that the lamellar spacing remained unchanged when processed with 7% DPE as additive. In addition, no matter the PBDT-TS1:H-tri-PDI blend films with or without DPE, both of them had the (010) diffraction peaks only in the out-of-plane direction, which demonstrated that a preferential face-on molecular orientation with respect to the substrate was formed in the blend films. What's more, the out-of-plane (010) coherence length of the blend films with and without DPE can be calculated via the Scherrer equation to be 2.1 and 1.7 nm, respectively. This declares that the higher crystallinity in the blend film can be achieved by using DPE as additive. These results indicated that the crystal in the blend films with 7% DPE became more perfect and the crystallinity as well as the π–π interaction was enhanced, which was beneficial to the charge transportation in the blend films.

In summary, a novel electron acceptor, H-tri-PDI is synthesized, characterized and employed as the electron acceptor in PSCs. Benefiting from the appropriate energy level alignment and the favorable morphology in PBDT-TS1:H-tri-PDI active layer, the J_{sc} of PSCs based on PBDT-TS1:H-tri-PDI is as high as 16.5 mA cm^{-2} and the PCE reaches to 7.25%, which is the highest value in the PSCs with H-*n*-PDI materials. The considerable results demonstrate that to link three PDI units via their imide positions is an effective method to make H-*n*-PDI be promising acceptor materials. In addition, the more active sites in H-*n*-PDI molecules provide more possibilities for further fine tuning their molecular energy levels and improving their charge carrier mobilities. Therefore, this work should have great significance in further promoting the development of new non-fullerene acceptor materials.

Supporting Information

Supporting Information is available from the Wiley Online Library or from the author.

Acknowledgements

N.L. and K.S. contributed equally to this work. The authors thank the support from the National Natural Science Foundation of China (NSFC) (21225209, 91427303, 91333204, 21190032, 21504006, 21534003), the 973 Program (2012CB932903 and 2014CB643502) and the Chinese Academy of Sciences (XDB12010100). X-ray data was acquired at beamlines 7.3.3 and 11.0.1.2 at the Advanced Light Source, which is supported by the Director, Office of Science, Office of Basic Energy Sciences, the U.S. Department of Energy under Contract No. DE-AC02-05CH11231.

Received: January 11, 2016
Revised: February 17, 2016
Published online:

[1] J. Chen, Y. Cao, *Acc. Chem. Res.* **2009**, *42*, 1709.
[2] Y. Li, *Acc. Chem. Res.* **2012**, *45*, 723.
[3] N. Sariciftci, L. Smilowitz, A. Heeger, F. Wudl, *Science* **1992**, *258*, 1474.
[4] C. Brabec, S. Gowrisanker, J. Halls, D. Laird, S. Jia, S. Williams, *Adv. Mater.* **2010**, *22*, 3839.
[5] H. Son, B. Carsten, I. Jung, L. Yu, *Energy Environ. Sci.* **2012**, *5*, 8158.
[6] L. Dou, J. You, J. Yang, C. Chen, Y. He, S. Murase, T. Moriarty, K. Emery, G. Li, Y. Yang, *Nat. Photonics* **2012**, *6*, 180.
[7] B. Thompson, J. Frechet, *Angew. Chem.* **2008**, *47*, 58.
[8] B. Kraabel, C. Lee, D. Mcbranch, D. Moses, N. Sariciftci, A. Heeger, *Chem. Phys. Lett.* **1993**, *213*, 389.
[9] J. van Franeker, M. Turbiez, W. Li, M. Wienk, R. Janssen, *Nat. Commun.* **2015**, *6*, 6229.
[10] A. Anctil, C. Babbitt, R. Raffaelle, B. Landi, *Environ. Sci. Technol.* **2011**, *45*, 2353.
[11] J. Halls, C. AWalsh, N. Greenham, E. Marseglia, R. Friend, S. Moratti, A. Holmes, *Nature* **1995**, *376*, 498.
[12] Y. Huang, E. Kramer, A. Heeger, G. Bazan, *Chem. Rev.* **2014**, *114*, 7006.
[13] Y. Liu, J. Zhao, Z. Li, C. Mu, W. Ma, H. Hu, K. Jiang, H. Lin, H. Ade, H. Yan, *Nat. Commun.* **2014**, *5*, 5293.
[14] S. Zhang, L. Ye, W. Zhao, B. Yang, Q. Wang, J. Hou, *Sci. Chin. Chem.* **2015**, *58*, 248.
[15] Z. He, B. Xiao, F. Liu, H. Wu, Y. Yang, S. Xiao, C. Wang, T. Russel, Y. Cao, *Nat. Photonics* **2015**, *9*, 174.
[16] G. Yu, J. Gao, J. Hummelen, F. Wudl, A. Heeger, *Science* **1995**, *270*, 1789.
[17] Z. Chen, A. Lohr, C. Saha-Moller, F. Wurthner, *Chem. Soc. Rev.* **2009**, *38*, 564.
[18] C. Li, H. Wonneberger, *Adv. Mater.* **2012**, *24*, 613.
[19] M. Li, L. Wang, J. Liu, K. Zhou, X. Yu, R. Xing, Y. Geng, Y. Han, *Phys. Chem. Chem. Phys.* **2014**, *16*, 4528.
[20] I. A. Howard, F. Laquai, P. Keivanidis, R. Friend, N. Greenham, *J. Phys. Chem. C* **2009**, *113*, 21225.
[21] X. Zhang, Z. Lu, L. Ye, C. Zhan, J. Hou, S. Zhang, B. Jiang, Y. Zhao, J. Huang, S. Zhang, Y. Liu, Q. Shi, Y. Liu, J. Yao, *Adv. Mater.* **2013**, *25*, 5791.
[22] X. Zhang, C. Zhan, J. Yao, *Chem. Mater.* **2015**, *27*, 166.
[23] J. Zhao, Y. Li, H. Lin, Y. Liu, K. Jiang, C. Mu, T. Ma, J. Lai, H. Hu, H. Yan, *Energy Environ. Sci.* **2015**, *8*, 520.
[24] D. Sun, D. Meng, Y. Cai, B. Fan, Y. Li, W. Jiang, L. Huo, Y. Sun, Z. Wang, *J. Am. Chem. Soc.* **2015**, *137*, 11156.
[25] Y. Zhong, M. Trinh, R. Chen, G. Purdum, P. Khlyabich, M. Sezen, S. Oh, H. Zhu, B. Fowler, B. Zhang, W. Wang, C. Nam, M. Sfeir, C. Black, M. Steigerwald, Y. Loo, F. Ng, X. Zhu, C. Nuckolls, *Nat. Commun.* **2015**, *6*, 8242.
[26] Y. Jiang, L. Lu, M. Yang, C. Zhan, Z. Xie, F. Verpoort, S. Xiao, *Polym. Chem.* **2013**, *4*, 5612.
[27] Y. Liu, C. Mu, K. Jiang, J. Zhao, Y. Li, L. Zhang, Z. Li, J. Lai, H. Hu, T. Ma, R. Hu, D. Yu, X. Huang, B. Tang, H. Yan, *Adv. Mater.* **2015**, *27*, 1015.

[28] Y. Lin, Y. Wang, J. Wang, J. Hou, Y. Li, D. Zhu, X. Zhan, *Adv. Mater.* **2014**, *26*, 5137.
[29] S. Rajaram, R. Shivanna, S. Kandappa, K. Narayan, *J. Phys. Chem. Lett.* **2012**, *3*, 2405.
[30] L. Ye, K. Sun, W. Jiang, S. Zhang, W. Zhao, H. Yao, Z. Wang, J. Hou, *ACS Appl. Mater. Interfaces* **2015**, *7*, 9274.
[31] C. Wu, C. Chueh, Y. Xi, H. Zhong, G. Gao, Z. Wang, L. Pozzo, T. Wen, A. Jen, *Adv. Funct. Mater.* **2015**, *25*, 5326.
[32] M. Thea, J. Michael, R. Michael, *J. Am. Chem. Soc.* **2009**, *131*, 8952.
[33] L. Heinz, J. Wolfgang, *Angew. Chem. Int. Ed.* **1998**, 37.
[34] J. Pommerehne, H. Vestweber, W. Guss, R. Mahrt, H. Bässler, M. Porsch, J. Daub, *Adv. Mater.* **1995**, *7*, 551.
[35] L. Ye, S. Zhang, W. Zhao, H. Yao, J. Hou, *Chem. Mater.* **2014**, *26*, 3603.
[36] S. Das, J. Keum, J. Browning, G. Gu, B. Yang, O. Dyck, C. Do, W. Chen, J. Chen, I. Ivanov, K. Hong, A. Rondinone, P. Joshi, D. Geohegan, G. Duscher, K. Xiao, *Nanoscale* **2015**, *7*, 15576.
[37] a) Z. Zheng, S. Zhang, M. Zhang, K. Zhao, L. Ye, Y. Chen, B. Yang, J. Hou, *Adv. Mater.* **2015**, *27*, 1189; b) Z. He, C. Zhong, S. Su, M. Xu, H. Wu, Y. Cao, *Nat. Photonics* **2012**, *9*, 591.
[38] a) Y. Zhong, M. Trinh, R. Chen, W. Wang, P. Khlyabich, B. Kumar, Q. Xu, C. Nam, M. Sfeir, C. Black, M. Steigerwald, Y. Loo, S. Xiao, F. Ng, X. Zhu, C. Nuckolls, *J. Am. Chem. Soc.* **2014**, *136*, 15215; b) Z. Zhang, H. Li, B. Qi, D. Chi, Z. Jin, Z. Qi, J. Hou, Y. Li, J. Wang, *J. Mater. Chem. A* **2013**, *1*, 9624.
[39] W. Ma, J. Tumbleston, M. Wang, E. Gann, F. Huang, H. Ade, *Adv. Energy Mater.* **2013**, *3*, 864.
[40] W. Ma, L. Ye, S. Zhang, J. Hou, H. Ade, *J. Mater. Chem. C* **2013**, *1*, 5023.
[41] B. Collins, Z. Li, J. Tumbleston, E. Gann, C. McNeill, H. Ade, *Adv. Energy Mater.* **2013**, *3*, 65.
[42] A. Hexemer, W. Bras, J. Glossinger, E. Schaible, E. Gann, R. Kirian, A. MacDowell, M. Church, B. Rude, H. Padmore, *J. Phys. Conf. Ser.* **2010**, *247*, 012007.
[43] E. Gann, A. T. Young, B. Collins, H. Yan, J. Nasiatka, H. Padmore, H. Ade, A. Hexemer, C. Wang, *Rev. Sci. Instrum.* **2012**, *83*, 045110.